# Hybrid spiropyran–silica nanoparticles with a core-shell structure: sol–gel synthesis and photochromic properties†

**Joachim Allouche,* Aurélie Le Beulze, Jean-Charles Dupin, Jean-Bernard Ledeuil, Sylvie Blanc and Danielle Gonbeau**

*Received 6th June 2010, Accepted 24th August 2010*
**DOI: 10.1039/c0jm01780a**

Photochromic hybrid spiropyran–silica nanoparticles with a core-shell structure were synthesized *via* a two step sol–gel procedure using tetraethoxysilane (TEOS) and methyltriethoxysilane (MTEOS) as silica precursors. The chemical nature and porosity of the materials were modified by the precursor ratio and the silylated spiropyran derivative chromophore was grafted and confined inside the nanoporous shell producing photoresponsive nanomaterials with a tunable dye photochromic response. When the MTEOS content increases in the matrices, the optical response was tuned from reverse to direct photochromism. Thermal bleaching after UV irradiation exhibits a blue shift of the reflectance maximum in the visible region assuming a modification of the dye populations towards open forms stabilized in more polar environments. The kinetic data were finally studied through a Gaussian model to evaluate the decay rates and to give an indication of the degree of heterogeneity of the materials.

## Introduction

Hybrid organic–inorganic photochromic materials have been the subject of many investigations over the past decade due to their potential applications, particularly in the design and development of optical switches or optical data storage devices.[1,2]

Such materials are characterized by their ability to undergo reversible changes in the visible absorption spectrum upon external stimuli, generally light or temperature.[3–5] In this field, the sol–gel process is a versatile route to trap an organic chromophore within an inorganic network and offers a control at the nanometric scale of the organic–inorganic hybrid nanostructure.[6] Among organic photochromic molecules, the spiropyran family is fascinating and is characterized by a light-induced heterolytic cleavage of the C–O bond producing the merocyanine form, the coloured isomer. Reversible isomerization to the closed spiropyran form is generally produced by thermal bleaching or visible light irradiation (Fig. 1).[7]

The main feature of the merocyanine is its possibility to interact with its environment (solvent, matrix) leading to various photochromic responses. Indeed, due to the zwitterionic structure of the coloured merocyanine form, polar environments induce negative photochromism with a blue shift of the absorption maximum. For more apolar environments, red shift is observed, resulting in positive photochromism. Negative and positive photochromism have been observed in solution,[8] as well as in sol–gel matrices.[9–13] Moreover, it is now well-known since the works of Levy and co-workers[9,10] that the coloured zwitterionic merocyanine form, when trapped into hydrophilic domains of a sol–gel silica matrix, tends to be stabilized through hydrogen bonding by residual acidic silanol groups. This effect results in the observation of reverse photochromism due to the stabilization of the coloured form without irradiation.[9,12,14,15] On the contrary, spiropyran embedded in a more hydrophobic network disfavours stabilization of the merocyanine form, which causes a so-called direct photochromism where the colourless form is stable without irradiation. The degree of heterogeneity of the matrix leads to different chemical environments where hydrophilic and hydrophobic domains produce a competition between reverse and direct photochromism with associated modulations of the absorption in the visible region.[16]

Design of new solid state optical devices with tunable optical responses requires a better understanding of the dye–matrix interactions and how confinement effects directly impact the photochromic properties. Such an approach needs sol–gel matrices with well-controlled structures with nanoscale-tunable chemical natures and dimensions. Previously, Yoon and co-workers[17,18] synthesized for the first time monodispersed core-shell silica nanoparticles with a structured mesoporous shell through a sol–gel procedure used recently by Blas *et al.*[19] and Audouin *et al.*[20] for the elaboration of mesoporous core-shell

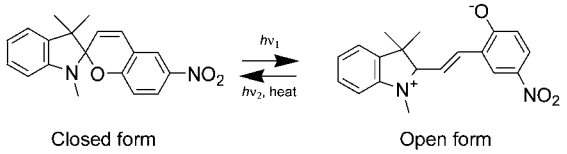


**Fig. 1** A representation of the photochromic closed and open forms of spiropyran.

*Université de Pau et des Pays de l'Adour (UPPA), UMR 5254 UPPA/CNRS Institut Pluridisciplinaire de Recherche sur l'Environnement et les Matériaux (IPREM), Equipe de Chimie Physique (ECP), Technopôle Hélioparc Pau Pyrénées, 2, Avenue du Président Pierre Angot, 64053 PAU Cedex 09, France. E-mail: joachim.allouche@univ-pau.fr; Fax: + 33 (0)5 59 40 76 22; Tel: +33 (0)5 40 17 50 75*

† This paper is part of a *Journal of Materials Chemistry* themed issue on Advanced Hybrid Materials, inspired by the symposium on Advanced Hybrid Materials: Stakes and Concepts, E-MRS 2010 meeting in Strasbourg. Guest editors: Pierre Rabu and Andreas Taubert.

 

nanocapsules. This procedure could be remarkably adapted to the design of new advanced hybrid systems for many applications since organic functionalization could be controlled and localized in the nanoporous shell. In this work, we give the first extension of this procedure through the elaboration of photoresponsive nanoparticles functionalized by spiropyran. We modified and adapted the synthesis conditions to the covalent grafting of spiropyran inside the matrix, which is an approach that has been seldom reported in the synthesis of spiropyran-silica based materials. The photochromic properties of spiropyran were tuned by varying the ratio of TEOS and MTEOS, the two silica precursors used in this study.

## Experimental

### Synthesis of spiropyran derivative 1′-(3-triethoxysilanpropyl)-3′-3′-dimethyl-nitrospiro[2*H*-1]benzopyran-2,2′-indoline (3)

(**3**) was synthesized by the direct reaction of 3′,3′-dimethyl-1′-(β-hydroxyethyl)-6-nitrospiro[2*H*-1-benzopyran-2,2′-indoline) (**1**) (TCI Europe, 1 g, 2.84 mmol) and 3-(triethoxysilyl)propyl isocyanate (**2**) (Sigma, 0.7 g, 2.82 mmol) in 20 ml of dry DMF at (80 °C) under nitrogen atmosphere for 7 h (Fig. 2).

$^1$H-NMR (400 MHz, $CDCl_3$), yield 63%, $\delta = 0.33$ (t, $J = 8.2$ Hz, 2H), 0.88 (t, $J = 7.1$ Hz, 9H), 0.93 (s, 6H), 1.38 (quint, $J = 8.2$ Hz, 2H), 2.8 (t, $J = 6.8$ Hz, 2H), 3.35 (dt, $J = 35$, 6.8 Hz, 2H), 3.48 (quad, $J = 6.9$ Hz, 6H), 3.97 (t, $J = 5.8$ Hz, 1H), 5.63 (d, $J = 10.4$ Hz, 1H), 6.39 (dd, $J = 8.2$, 1.9 Hz, 1H), 6.49 (td, $J = 7.5$, 0.9 Hz, 1H), 6.63 (d, $J = 10.3$ Hz, 1H), 6.73 (dd, $J = 7.2$, 1.1 Hz, 1H), 6.81 (td, $J = 7.6$, 1.3 Hz, 1H), 6.80 (d, $J = 7.6$ Hz, 1H), 7.77 (dd, $J = 8.8$, 2.8 Hz, 1H).

The solution obtained, with a concentration of spiropyran derivative of $9\times10^{-2}$ M, was protected from light and directly used for the synthesis of hybrid nanoparticles.

### Nanoparticles preparation

**Synthesis of dense core silica nanoparticles (CN).** Core silica nanoparticles were prepared by a typical Stöber method using tetraethoxysilane (TEOS, Aldrich) as the silica precursor in an alkaline solution. A mixture of 100 ml of ethanol (Fluka), 8 ml of deionized water and 2 ml of concentrated ammonia solution (28–30%, Aldrich) was prepared. To this mixture, TEOS (6 ml) was slowly added and reaction was performed at room temperature overnight. The TEOS : $NH_3$ : EtOH : $H_2O$ molar ratio was 1 : 1.14 : 64.7 : 19.2. This stock nanoparticles suspension was kept at room temperature before use.

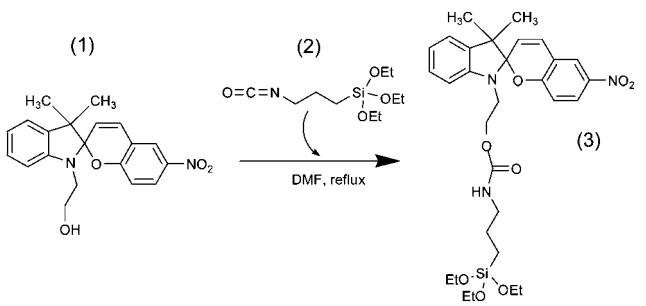


**Fig. 2** The silylation of hydroxyethyl-spiropyran. The as-prepared red solution was characterized by $^1$H-NMR to check for the presence of the urethane linkage and complete consumption of isocyanate.

**Synthesis of porous hybrid nanoparticles (HNP) with different silica precursors.** The previously synthesized CN core nanoparticles were surrounded by a porous hybrid shell using a "one pot" co-condensation method as follows: 0.241 g of cetyltrimethylammonium bromide (CTAB, Aldrich) as surfactant was first dissolved in a solution of 45.6 ml of water and 19.2 ml of ethanol. 20 ml of the CN suspension was then poured in this solution and stirred for 30 min at room temperature. To this suspension, 0.427 ml of the spiropyran derivative (**3**) solution was slowly added with either 0.429 ml of TEOS, 0.383 ml of methyltriethoxysilane (MTEOS, Aldrich)), or 0.214 ml of TEOS and 0.191 ml of MTEOS in order to obtain three materials with TEOS : MTEOS molar ratios of 100 : 0, 0 : 100 or 50 : 50. The materials were labelled HNP-T, HNP-M and HNP-MT respectively. For this step, the PRECURSORS : CTAB : $NH_3$ : EtOH : $H_2O$ : (3) molar ratio is 1 : 0.34 : 2.75 : 171 : 1320 : 0.02. The reaction was left to proceed overnight at room temperature.

From this protocol, calculation of the theoretical dye concentration in the shell gives $3.3\times10^{-4}$ mol $g^{-1}$ *i.e.* $2\times10^{20}$ dye molecules per g of silica in the shell.

For comparison, the same protocol was used for the preparation of reference dye-free materials, which are denoted as NP-T, NP-M and NP-MT.

For all cases, the nanoparticles were recovered by filtration and washed copiously with ethanol and acetone before drying overnight at 80 °C. The powders were resuspended in a HCl (1 M)/EtOH solution and stirred for 12 h to eliminate the surfactant. The nanoparticles were recovered by a second filtration, washed several times by ethanol and acetone, and finally dried at 80 °C overnight.

### Characterizations

The diameters of the core particles were measured by dynamic light scattering (DLS) using a CORDOUAN VASCO-2 particle size analyser (laser diode 658 nm, 75 mW) in ethanol at 20 °C.

Transmission electron microscopy (TEM) images were taken with a Philips CM 200 (200 kV) instrument equipped with a LaB6 source. The samples dispersed in ethanol were dropped onto a carbon copper grid and dried before analysis.

Scanning electron microscopy (SEM) pictures were performed on a JEOL JAMP-9500F Field Emission Auger Microprobe operating at 10 kV and 5 nA. The powders were placed on carbon adhesive before being mounted on the sample microscope holder.

Nitrogen adsorption and desorption isotherms of the nanoparticles were measured at 77 K on a Micromeritics ASAP 2010 nitrogen adsorption apparatus. Surface area values were obtained with the corrected Brunauer–Emmet–Teller (BET) equation. Median pore diameters were calculated from a Barrett–Joyner–Halenda (BJH) model for mesoporous materials or a Horvath–Kawazoe (HK) model for microporous materials.[21]

DRIFT spectra were collected on a Magna 560 Nicolet spectrometer purged with dried air, with a resolution of 4 $cm^{-1}$ after signal averaging of 200 scans.

XPS measurements were performed on a Thermo K-alpha spectrometer with a hemispherical analyzer and a microfocussed (microspot 400 μm diameter) monochromated radiation (Al Kα, 1486.6 eV) operating at 72 W under a residual pressure of $1 \times 10^{-9}$ mbar. The pass energy was set to 40 eV. Charge effects were compensated by the use of a dual beam charge neutralisation system (low energy electrons and $Ar^+$ ions), which had the unique ability to provide consistent charge compensation. All the neutraliser parameters remained constant during analysis and allow one to find a 285.0 eV C1s binding energy for adventitious carbon. Spectra were mathematically fitted with Casa XPS software using a least squares algorithm and a non-linear baseline. The fitting peaks of the experimental curves were defined by a combination of Gaussian (70%) and Lorentzian (30%) distributions.

UV/vis diffuse reflectance spectra were recorded on a double beam Cary 5000 spectrophotometer in steps of 1 nm in the range 280–700 nm using an 11 cm diameter integrating sphere with a custom-made powder holder. Thermal decolouration in the dark of the powders was recorded after their irradiation under 4 UV lamps (PHILIPS TLD 15W/05) over 5 min. The diffuse reflectance spectra were recorded at fixed time intervals in dark and were corrected *versus* a white standard (Teflon, Aldrich, 55 μm)[22] and analyzed according to the Kubelka–Munk model.[23]

## Results and discussion

### Materials synthesis

The hybrid nanomaterials were synthesized *via* a two step sol–gel method based on a dual-templating process inspired from a protocol developed, previously.[19,20] During the first step, the core nanoparticles (CN) were synthesized according to a typical Stöber process in alkaline medium.[24] In the second step, the CN particles act as core templating materials and nucleation sites for the growth of the shell. CTAB is used as the second templating agent to structure the shell porosity. Electrostatic interactions between the negatively charged surface of the silica CN particles and the positively charged surfactant molecules favoured the silica polymerization on the particles surface to finally obtain a well-defined core-shell structure. Without being above the CMC in the reaction solution, the porosity is induced by a cooperative effect between silicate condensation, which locally promotes an excess of negatively charged silicates at the CN nanoparticles surface. This excess of charge is compensated by an increasing concentration of surfactant giving micellar structures in the native solid state materials. In our case, we adapted the synthesis conditions to the grafting of a silylated spiropyran derivative inside the porous shell. The silylation of the spiropyran allowed us to introduce the dye in the reaction medium during the shell formation. Hybridisation of the shell took place due to the simultaneous and combined hydrolysis-condensation reactions of the silica precursors and of the silylated part of the dye. This so-called "one-pot" method was chosen to provide a more homogeneous dispersion of the dye in the nanostructure in comparison to a classical post-synthesis grafting.[25] Moreover, in our case, we used two types of silica precursors to modify the chemical nature of the mesoporous shell and consequently the photochromic properties of the dye.

### Microscopic characterization

TEM and SEM pictures of the nanomaterials are depicted in Fig. 3. CN particles (Fig. 3a) show well-dispersed particles with diameters around 130 nm which are in agreement with the DLS data (inset) giving a narrow size distribution centered at 133 nm. Low and high magnification pictures in Fig. 3c–h correspond to the hybrid dye–silica HNP-M, HNP-MT and HNP-T nanomaterials. The low magnification images exhibit homogeneous particle sizes with some aggregation, but with a clearly visible core-shell structure, which is confirmed by the SEM image of HNP-T (Fig. 3b) where broken nanoparticles (showed by arrows) are obviously identifiable.

Higher magnification pictures reveal that the core-shell morphology depends on the samples. The shell thickness, evaluated at 24 nm, 23 nm and 14 nm for HNP-T, HNP-MT and HNP-M respectively, decreases with the increase of the MTEOS content in the nanostructure. This result was attributed to the diminution of pore sizes due to the inclusion of methyl groups when MTEOS is used for the synthesis.[26]

### Nitrogen adsoption-desorption analysis

Nitrogen adsorption and desorption measurements confirm this observation. Isotherms of non-grafted materials NP-T, NP-MT and NP-M as well as hybrid dye–silica nanoparticles HNP-T and HNP-MT are depicted in Fig. 4. For HNP-M, data measurements were inaccurate probably because of the weak nitrogen–adsorbent interactions caused by a high content of organic groups on the material surface. Isotherms of pure TEOS nanoparticles (NP-T and HNP-T) exhibit a typical type IV behaviour,

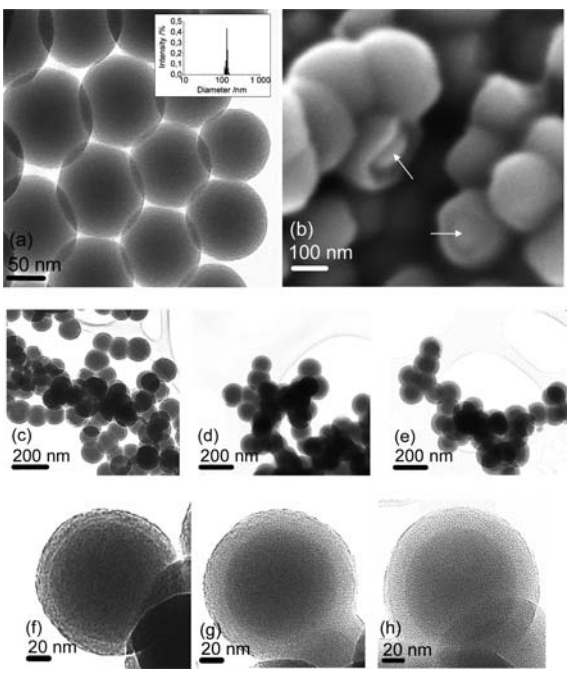


**Fig. 3** TEM and SEM pictures of silica core and hybrid nanoparticles. (a) A TEM picture of CN nanoparticles with, in the inset, the corresponding size distribution; (b) a SEM picture of HNP-T; (c) and (f), (d) and (g), (e) and (h) show low and high magnification TEM pictures of HNP-M, HNP-MT and HNM-T, respectively.

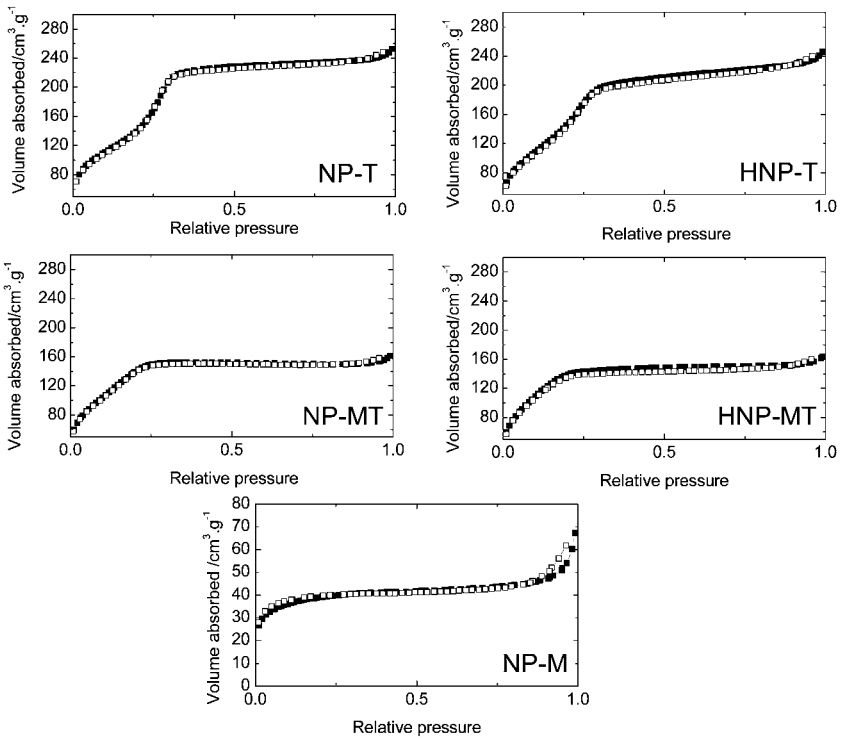


**Fig. 4** Nitrogen absorption and desorption isotherms of reference (spiropyran-free) and hybrid spiropyran–silica nanoparticles.

which is characteristic of mesoporous materials. For pure MTEOS nanoparticles *i.e.* NP-M, the isotherm shape is associated to a type I behaviour, which corresponds to microporous materials.[26] A slight hysteresis can also be observed for NP-M that we assigned to a delayed capillary condensation caused by particles aggregation.[27] For mixed TEOS/MTEOS matrices, NP-MT and HNP-MT, isotherms reveal combined type I and type IV behaviours indicating that micro- and mesopores are present in the material.

BET surface areas and median pore diameters deducted from isotherms have been reported in Table 1. Due to their microporous structure, the NP-M nanoparticles exhibit the lowest surface area (144 $m^2\ g^{-1}$) and lowest median pore diameter (1.3 nm). On the other hand, mixed TEOS/MTEOS matrices, NP-MT and HNP-MT, present higher areas than the corresponding pure TEOS nanoparticles, NP-T and HNP-T. This can be explained by their combined micro- and mesoporosity giving a more heterogenous structure and higher surface areas. Moreover, the surface areas are higher for HNP than for NP, suggesting that the sol–gel nanostructures were altered by spiropyran which induces a modification of the inorganic network organization.[28a] Finally, the decrease in pore diameters with the inclusion in the matrices of organic groups, spiropyran or methyl groups from MTEOS is associated to the pore filling process.[28b]

**Table 1** BET surface area and median pore diameters of reference (dye-free) and hybrid nanoparticles

| | BET surface area/$m^2\ g^{-1}$ | | | Median pore diameter/nm | | |
|---|---|---|---|---|---|---|
| Labels<br>Materials | T | MT | M | T | MT | M |
| NP | 506 | 535 | 144 | 2.2 | 1.7[a]<br>1.4[b] | 1.3[b] |
| HNP | 538 | 555 | — | 2 | 1.6[a]<br>1.35[b] | — |

[a] Calculated from the BJH model. [b] Calculated from the HK model.

## DRIFT characterization

DRIFT spectra of hybrid HNP-T, HNP-M and HNP-MT nanoparticles showed in Fig. 5 confirm the encapsulation of spiropyran in the matrices although the low dye concentration compared to the silica signal did not allow the identification of all spiropyran groups. The spectra exhibit a broad band at 1640–1702 $cm^{-1}$ assigned to the amide group of the spiropyran derivative.[29–31] This band is more pronounced in TEOS-containing

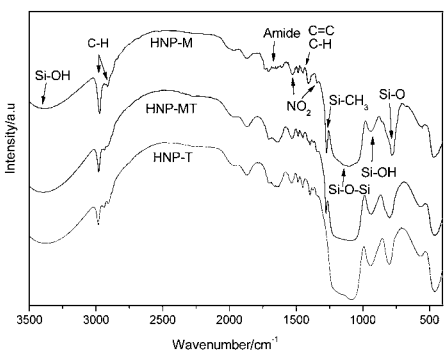


**Fig. 5** DRIFT spectra of HNP-M, HNP-MT and HNP-T nanoparticles.

material due to the overlapping signal of adsorbed water. On the other hand, the two peaks at 1344 $cm^{-1}$ and 1529 $cm^{-1}$ were attributed to the stretching vibrations of the aryl nitro group[32] whereas, in the 1405–1495 $cm^{-1}$ region, peaks were attributed to C═C aromatic and C–H alkyl bonds vibrations. The strong absorption denoted at 1090–1230 $cm^{-1}$ and the peak at 797 $cm^{-1}$ correspond to Si–O–Si and Si–O stretching vibrations, respectively.[30] A sharp peak at 940 $cm^{-1}$, which decreases with the increase of the MTEOS content and a broad absorption at 3400 $cm^{-1}$ are equally present. These contributions were assigned to the Si–OH stretching vibrations.[30,33] In addition, a sharp peak at 1276 $cm^{-1}$, not visible for HNP-T, appears for HNP-MT and HNP-M, and represents the Si–$CH_3$ bending.[33] This peak increases with the MTEOS content as well as the bands below 3000 $cm^{-1}$ corresponding to alkyl C–H alkyl vibrations.

## XPS analysis

To better appreciate the chemical structure of the core-shell modified silica materials, X-ray photoelectron spectroscopy (XPS) analyses were carried out on commercial dye hydroxyethyl-spiropyran (**1**), on the silylated spiropyran derivative (**3**), on the silica core-shell nanoparticles (NP-T, NP-M and NP-MT) and on the three hybrid systems (HNP-T, HNP-M and HNP-MT).

For the photochromic hydroxyethyl–spiropyran commercial dye (**1**), high-resolution spectra were recorded in the regions of C1s, O1s and N1s and were compared to the literature.[34]

The different atomic concentrations match the chemical formula of the dye (number of atoms) as the C/O and O/N theoretical and experimental atomic ratios are nearly the same (respectively 4.9 [theo. = 5] and 2.3 [theo. = 2]). Moreover, the close-up survey of the O1s and N1s spectra indicates the co-existence of the open and closed forms of the dye powder under the analysis conditions. For the N1s spectrum (Fig. 6a), the two conformers in equilibrium distinguishing themselves with the components at 399.3 eV (3.1 at.%, amine nitrogen, closed form) and 400.4 eV (0.6 at.%, ammonium nitrogen, open form).

Simultaneously, the presence of a small component at 530.1 eV on the O1s spectrum (Fig. 6b) is observed in the same proportion as the ammonium N1s one (0.6 at.%), which perfectly assumes, in minority, the open form signature. On the high energy side of the N1s region, the component at 405.7 eV corresponds to the nitro functional group (3.0 at.%). It is to be noted that some traces of water were found in the commercial dye powder (O1s = 534.3 eV).

Before its insertion within the shell of the inorganic silica host, the photochromic dye was modified with the grafting of a functional arm for the anchorage in the mineral pores (silylated spiropyran derivative, molecule (**3**) in Fig. 2). The precise resolution of the XPS was even in this case an adapted probe to check this chemical modification. For example, the C/O, Si/N and O/Si atomic ratios were found in the expected ranges of data with values of 3.5 (theo. = 3.75), 0.39 (theo. = 0.33) and 7.4 (theo. = 8.0), respectively. The new component observed in the C1s spectrum at 289.3 eV (Fig. 7) is another evidence of the functionalization, as it is assigned to R–HN–(C═O)O–R′ carbamate carbon atoms with a $C_{carbamate}$/N atomic ratio of 0.37 (theor.: 0.33). In addition, the presence of a Si2p peak at 102.4 eV attests to the presence of the $Si(OEt)_3$ group.

Core-shell reference materials NP-T, NP-M and NP-MT were also fully-characterized with XPS and according to the precursors used in their preparation, TEOS, MTEOS or MTEOS/TEOS, the binding energy of the Si2p peak was recorded at 103.8 eV, 103.1 eV and 103.4 eV, the last value being intermediate between the two previous ones according to the 50/50 MTEOS/TEOS mixture used. It is to be noted that these values are consistent with the expected evolution of the polarity matrix. Quantitative analysis has confirmed the expected atomic arrangement in these core shell systems with O/Si ratios around 2.5 for NP-T (theor. = 2.0), 1.6(5) for NP-M (theor. = 1.5) and 2.0 for NP-MT. The carbon content also agrees with the expected trend according to the precursors used (~10 at.% for NP-T, ~32 at.% for NP-M and ~18.5 at.% for NP-MT). In addition, no nitrogen signal was recorded on these materials confirming the complete elimination of the CTAB template after washing the matrices.

The hybrid systems HNP-T, HNP-M and HNP-MT were analysed by XPS under the same conditions. The first observations indicated a preserved silica environment in all cases with nearly the same Si2p binding energies and O/Si ratios as previously (Table 2). At the surface of the materials, the process of organic confinement in pores seems to be effective as a clear N1s signal is recorded for the three hybrids (0.5–1.0 at.%). Besides, carbon contents in the same range, as previously, are recorded for HNP-T and HNP-MT, respectively at 12.9 at.% and 22.8 at.%. Simultaneously, similar Si2p binding energy (103.6 eV) suggests the same silicon chemical environment at the shell surface. In the case of the HNP-T, the N1s signal allows one to fit the experimental profile into two components at 399.7 eV (carbamate nitrogen and amine nitrogen of closed form) and 401.7 eV (ammonium nitrogen of open form) in agreement with

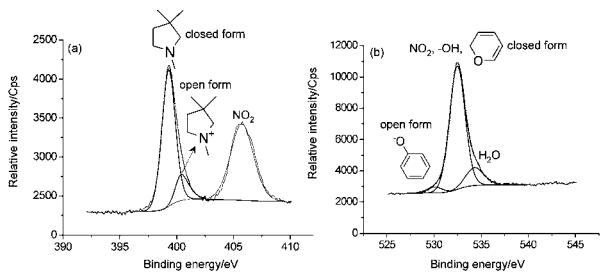


**Fig. 6** XPS spectra of the hydroxyethyl–spiropyran dye: (a) N1s and (b) O1s.

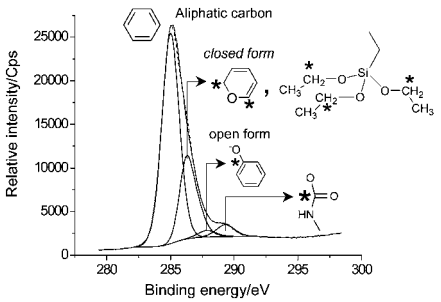


**Fig. 7** The C1s XPS spectrum of the silylated spiropyran dye (**3**).

**Table 2** The XPS composition table of reference dye-free materials and hybrid nanoparticles with the corresponding binding energies assignation of the Si2p core level, the O/Si ratios and carbon amount

| | NP-T | NP-M | NP-MT | HNP-T | HNP-M | HNP-MT |
|---|---|---|---|---|---|---|
| Si2p (eV) | 103.8 | 103.1 | 103.4 | 103.6 | 103.5 | 103.5 |
| O/Si | 2.5 | 1.6(5) | 2.0 | 2.4 | 1.6(5) | 1.9(5) |
| C (at.%) | 10.1 | 32.1 | 18.4 | 12.9 | 35.7 | 22.8 |

the color of this hybrid material. In addition, the $C_{carbamate}/N$ ratio is calculated to be 0.35, then the integrity of the silylated dye after grafting in the inorganic silica pores is preserved. The same conclusions can be made for HNP-MT with $C_{carbamate}/N = 0.29$. Concerning the HNP-M hybrid nanoparticles, the high content of carbon (35.7 at.%) prevents one to detect, in the limit of resolution, any carbamate signal. Moreover, the N1s spectrum is decomposed in a single component corresponding to the absence of the silylated dye open form.

## Photochromic properties

After equilibration of the hybrid materials in the dark and before irradiation, the powders are pink, but lightly coloured. The color is more intense as the content of TEOS in the matrices increases. This observation is corroborated by the UV-vis diffuse reflectance spectra before irradiation in Fig. 8. For all samples, the reflectance intensity in the visible region indicates that spiropyran presents an open form in the dark. However, this intensity increases proportionally to the content of TEOS in the materials. This result indicates that, as the polarity of the matrix increases, the merocyanine form is probably stabilized by strong hydrogen bonds *via* silanol fragments. Moreover, we note a blue shift of the maximum in this region with the increase of the matrix polarity reflecting a negative photochromism typical of the zwitterionic form behaviour of the merocyanine. The maxima are located at 543, 530 and 525 nm for HNP-M, HNP-MT and HNP-T respectively indicating a highest blue shift for the most polar HNP-T matrix. At shorter wavelengths near 400 nm, we note especially for HNP-T another absorption band attributed to the formation of protonated merocyanine forms, which is an indication of strong acidic environments surrounding the dye.[16,35] After 5 min UV irradiation at 350 nm, the materials exhibit complex and different photochromic behaviours depending on the chemical nature of the hybrid materials.

For HNP-T, irradiation produces bleaching with a decrease of intensity and a red shift of the maximum from 525 nm to 546 nm (Fig.9).

After irradiation, slow colouration occurs over 200 min with a blue shift of the maximum to 525 nm, the same wavelength value as before irradiation. This result can be attributed to typical reverse photochromism behaviour, where the open form stabilized by strong hydrogen bonds reverts back to the closed form under the action of light. The return to the open stabilized form involves negative photochromism with a displacement of the intensity maximum towards lower wavelengths. This reflects a particular behaviour for which dye populations are progressively influenced by the matrix polarity when stabilization of the open zwitterionic form is occurring.

On the contrary, for HNP-M and HNP-MT, irradiation produces intense colourations implying the opening reaction of spiropyran (Fig. 10). The intensity of the reflectance maximum just after irradiation decreases with polarity of the matrix, involving a more intense colouration for the pure MTEOS material (HNP-M) than for the mixed TEOS/MTEOS material (HNP-MT). Moreover, comparing the $\lambda_{max}$ values in the visible region before and after irradiation, we note a red shift from $\lambda_{max} = 543$ nm and 530 nm (see Fig. 8) to $\lambda_{max} = 580$ nm and 564 nm for HNP-M and HNP-MT respectively. Higher $\lambda_{max}$ for HNP-M than for HNP-MT after irradiation denotes a globally higher apolar nanostructure for the pure MTEOS materials resulting in a more pronounced red shift of the reflectance maximum.

Studying the thermal back reaction after irradiation, an important blue shift occurs after 200 min until $\lambda_{max} = 567$ nm and 540 nm for HNP-M and HNP-MT respectively. Such a phenomenon was previously observed with spiropyran trapped within an organogel matrix.[36] The authors assigned this change of the absorption profile over time to the existence of open merocyanine forms in different environments. A similar explanation could be made for our hybrid materials and developed as follows.

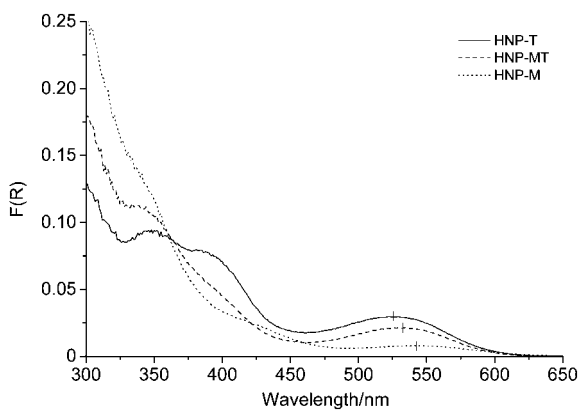


**Fig. 8** UV-vis diffuse reflectance spectra of hybrid spiropyran–silica nanoparticles before irradiation after 15 days in dark.

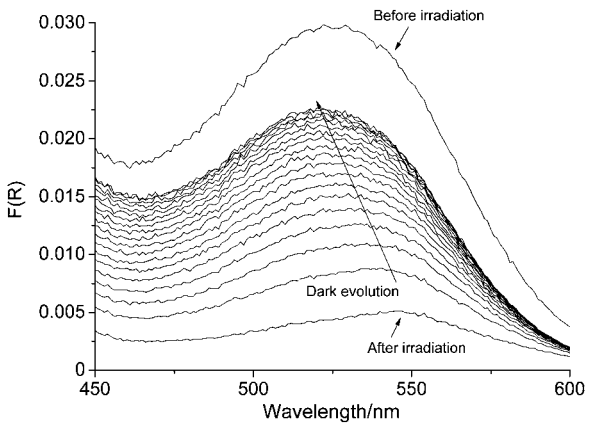


**Fig. 9** The dark evolution of the UV-vis diffuse reflectance spectra of HNP-T nanoparticles after irradiation.

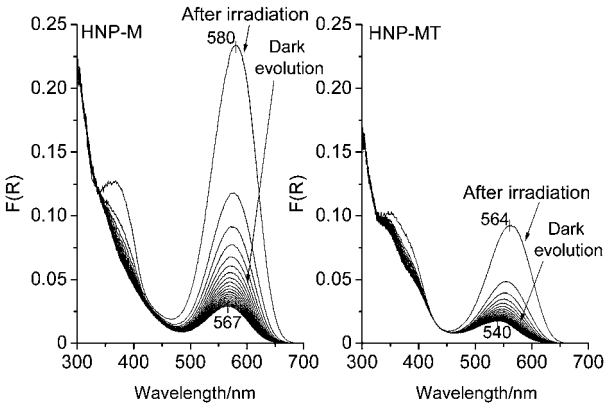


**Fig. 10** The dark evolution of the UV-vis diffuse reflectance spectra of HNP-M and HNP-MT nanoparticles after UV irradiation at 350 nm during 5 min.

First, the degree of dispersion of the dye in the host materials has to be evaluated from the BET analysis, XPS data and on the basis of the theoretical dye concentration in the shell (see experimental section). The average density of dye in the shell was estimated to 0.2 molecules $nm^{-2}$ for HNP-T and HNP-MT, and 0.75 molecules $nm^{-2}$ for HNP-M. Considering the dimensions of a dye molecule (1.7 nm length and 0.7 nm width) as well as their surface coverage of around 1.14 $nm^2$,[37] the average distance between the dye molecules in the host materials can be evaluated between 2 and 4 nm, which is smaller than 6 nm, the distance obtained for Förster quenching in solvent or molecular sieves.[35a,38] Thus, we cannot exclude a possible self-quenching of the dye molecules in the hybrid materials. Fluorescence characterizations will be conducted to elucidate this point. However, according to the pore sizes measured (<2.2 nm), the large dye molecules fill the pores in a high extent and we consider in the next discussion that the dye optical properties are preferentially influenced by the matrix.

The heterogeneous structure of the materials leads to a distribution of sites of localized steric and chemical constraints to the ring opening or closing reactions impacting directly the photochromic responses of the trapped dyes. The global optical response of the material can be defined as the sum of contributions of each photochromic response linked to a dye population placed in specific interactions with the matrix. Following this explanation, we assumed that the blue shift observed for HNP-M and HNP-MT is due to a modification of the merocyanine populations over time from those trapped in less polar environments towards those that are better stabilized in more polar environments. Consequently, the blue shift can be considered as an indication of the distribution of dye populations within the matrix directly linked to the dispersion of environments and consequently to the degree of heterogeneity of the material.

To reinforce this assumption, we analysed the thermal bleaching kinetics through a Gaussian model developed specifically for heterogeneous systems by Albery *et al.*,[39] applied for the first time on a porous silica matrix by Samuel and co-workers[40] and extended to the spirooxazines–silica interactions by Biteau *et al.*[16,41] This model leads to better fits for photochromic materials based on silica matrices than the classical biexponential model and allows a good description of the degree of heterogeneity of materials, as well. In addition, to our knowledge, it is the first time that this model has been used to characterize the thermal bleaching of spiropyrans grafted on a mesoporous silica matrix. The Gaussian model is based on a normal distribution of free energies leading to a Gaussian distribution of $\ln(k)$, where $k$ is defined as the decay rate constant of the thermal bleaching. The Gaussian distribution of $\ln(k)$ is centered around $\ln(k_{av})$, where $k_{av}$ is the average rate constant of the reaction. The two fitting parameters are $k_{av}$ and $\gamma$, the dispersion of the Gaussian in $\ln(k)$ giving a quantitative estimation of the extent of heterogeneity of the matrix. The model could not be applied to the

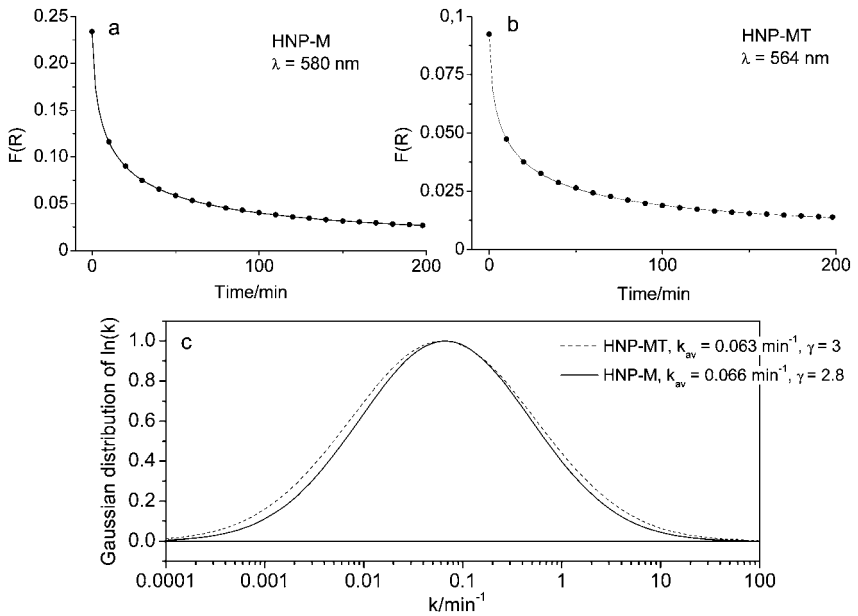


**Fig. 11** (a) The F(R) decays for HNP-M at $\lambda = 580$ nm; (b) F(R) decays for HNP-MT at $\lambda = 564$ nm; (c) Gaussian distributions of $\ln(k)$ deduced from the fits for HNP-M and HNP-MT with the corresponding fitting parameters.

 

HNP-T material due to the reverse photochromism behaviour implying no thermal bleaching in dark.

Kinetic data of the reflectance intensity decays were analyzed and taken at wavelengths corresponding to the maxima just after irradiation *i.e.* $\lambda = 580$ nm and $\lambda = 564$ nm for HNP-M and HNP-MT respectively. Fig. 11 displays excellent agreement between the model and the experimental decays of HNP-M (Fig. 11a) and HNP-MT (Fig. 11b). The parameters $k_{av}$ and $\gamma$ were deduced from the fit for each of the samples and the Gaussian distributions in $\ln(k)$ are reported in Fig. 11c with the values of the two fitting parameters.

We note for HNP-M and HNP-MT similar values of $k_{av}$ of around 0.06 $min^{-1}$ suggesting that the average decay rate is not affected by the chemical nature of the materials. This result reflects only that the chemical nature between the two matrices does not differ sufficiently to observe a significant influence on the decay rate through this Gaussian model. However, the comparison of the $\gamma$ parameter denotes a lower value for HNP-M than for HNP-MT suggesting a larger degree of heterogeneity for HNP-MT. This could reflect that using two precursors leads to a higher heterogeneity than for the pure MTEOS materials. This result can be put in relation with the blue shifts observed in Fig. 10 where a larger wavelength gap is observed during thermal bleaching for HNP-MT (24 nm) than for HNP-M (13 nm) suggesting that, in the first case, the open merocyanine forms are embedded in a broader distribution of chemical environments in relation to a higher heterogeneous structure of the host.

## Conclusion

Hybrid spiropyran–silica nanoparticles with core-shell structure were synthesized *via* a dual templating sol–gel method using two different precursors, TEOS and MTEOS. Grafting of the silylated dye was carried out by a "one-pot method" during the shell growth. The materials show different nanostructures and chemical organizations depending on the TEOS/MTEOS ratio used for the synthesis. Diminution of the nanoparticles shell thickness is related to the reduction of the pore sizes from a mesoporous structure for HNP-T towards a microporous organization for HNP-M. XPS analysis allows one to probe chemical nature of the materials and it showed a progressive reduction of the Si2p binding energies and of the O/Si ratio, as well as an increase in the carbon amount with the MTEOS content. This suggests a clear trend to an apolar structure when this precursor is used. In addition, detection of nitrogen and carbon carbamate signals, in adequate proportions, attests to a preservation and of an effective grafting of the dye within the hosts.

Optical experiments revealed a very high sensitivity of the photochromic behaviour of spiropyran to the chemical nature of the materials. Reverse photochromism was observed for the most polar matrix (HNP-T), whereas direct photochromism was associated to the more apolar materials (HNP-M and HNP-MT). After irradiation, HNP-T exhibited colouration in the dark with a blue shift of the reflectance maximum indicating a progressive strong stabilization of the open merocyanine placed in higher polar environments. On the other hand, HNP-M and HNP-MT show thermal bleaching with a blue shift characteristic of a change of the merocyanine populations over time from less stabilized ones in apolar environments towards better stabilized ones in polar environments. The comparison of the wavelength gaps during thermal bleaching of HNP-M and HNP-MT suggests a broader distribution of chemical environments in the latter case. This result is consistent with the study of kinetic data through a Gaussian model, which suggests a higher degree of heterogeneity for HNP-MT made from mixed silica precursors.

## Acknowledgements

We would like to acknowledge the IPREM-EPCP team and Abdel Khoukh for the NMR experiments and interpretation. We thank F. Portail, C. Bessibes, and F. Casbas of Arkema Industry for the TEM analysis realized on the materials. We also thank region Aquitaine for financial support to our lab.

## Notes and references

1 C. Sanchez, B. Lebeau, F. Chaput and J.-P. Boilot, *Adv. Mater.*, 2003, **15**, 1969–1994.
2 M.-S. Wang, G. Xu, Z.-J. Zhang and G.-C. Guo, *Chem. Commun.*, 2010, **46**, 361–376.
3 H. Bouas-Laurent and H. Dürr, *Pure Appl. Chem.*, 2001, **73**, 639–665.
4 J. C. Crano and R. J. Guglielmetti, *Organic Photochromic and Thermochromic Compounds*, Vol. 1, Plenum, New York, 1999.
5 J. C. Crano and R. J. Guglielmetti, *Organic Photochromic and Thermochromic Compounds*, Vol. 2, Plenum, New York, 1999.
6 C. Sanchez, B. Julián, P. Belleville and M. Popall, *J. Mater. Chem.*, 2005, **15**, 3559–3592.
7 R. Guglielmetti, in *Photochromism, Molecules and Systems*, ed. H. Dürr and H. Bouas-Laurent, Elsevier, Amsterdam, 2003, p. 314–455.
8 J. B. Flannery Jr, *J. Am. Chem. Soc.*, 1968, **90**, 5660–5671; N. W. Tyer Jr and R. S. Becker, *J. Am. Chem. Soc.*, 1970, **92**, 1295–1302; A. S. Kholmanskii, A. Z. Zubkov and K. M. Dyumaev, *Russ. Chem. Rev.*, 1981, **50**, 305–315; A. S. Kholmanskii and K. M. Dyumaev, *Russ. Chem. Rev.*, 1987, **56**, 136–151; S.-R. Keum, M.-S. Hur, P. M. Kazmaier and E. Buncel, *Can. J. Chem.*, 1991, **69**, 1940–1947; A. K. Chibisov and H. Görner, *Chem. Phys.*, 1998, **237**, 425–442.
9 D. Levy and D. Avnir, *J. Phys. Chem.*, 1988, **92**, 4734–4738.
10 D. Levy, S. Einhorn and D. Avnir, *J. Non-Cryst. Solids*, 1989, **113**, 137–145.
11 G. Wirnsberger, B. J. Scott, B. F. Chmelka and G. D. Stucky, *Adv. Mater.*, 2000, **12**, 1450–1454.
12 A. Leaustic, A. Dupont, P. Yu and R. Clement, *New J. Chem.*, 2001, **25**, 1297–1301.
13 N. Andersson, P. Alberius, J. Örtegren, M. Lindgren and L. Bergström, *J. Mater. Chem.*, 2005, **15**, 3507–3513.
14 B. Schaudel, C. Guermeur, C. Sanchez, K. Nakatani and J. A. Delaire, *J. Mater. Chem.*, 1997, **7**, 61–65.
15 I. Casades, M. Alvaro, H. Garcia and M. N. Pillai, *Photochem. Photobiol. Sci.*, 2002, **1**, 219–223.
16 J. Biteau, F. Chaput and J.-P. Boilot, *J. Phys. Chem.*, 1996, **100**, 9024–9031.
17 S. B. Yoon, J.-Y. Kim, J. H. Kim, Y. J. Park, K. R. Yoon, S.-K. Park and J.-S. Yu, *J. Mater. Chem.*, 2007, **17**, 1758–1761.
18 J. H. Kim, S. B. Yoon, J.-Y. Kim, Y. B. Chae and J.-S. Yu, *Colloids Surf., A*, 2008, **313–314**, 77–81.
19 H. Blas, M. Save, P. Pasetto, C. Boissiére, C. Sanchez and B. Charleux, *Langmuir*, 2008, **24**, 13132–13137.
20 F. Audouin, H. Blas, P. Pasetto, P. Beaunier, C. Boissière, C. Sanchez, M. Save and B. Charleux, *Macromol. Rapid Commun.*, 2008, **29**, 914–921.
21 F. Rouquerol, J. Rouquerol and K. Sing, *Adsorption by Powders and Porous Solids*, Academic Press, London, 1999.
22 V. R. Weidner and J. J. J Hsia, *J. Opt. Soc. Am.*, 1981, **71**, 856–861.
23 P. Kubelka and F. Z. Munk, *Tech. Phys.*, 1931, **12**, 593–601.
24 W. Stöber, A. Fink and E. Bohn, *J. Colloid Interface Sci.*, 1968, **26**, 62–69.
25 M. H. Lim and A. Stein, *Chem. Mater.*, 1999, **11**, 3285–3295.

26 M. Kruk, T. Asefa, N. Coombs, M. Jaroniec and G. A. Ozin, *J. Mater. Chem.*, 2002, **12**, 3452–3457.
27 F. Rouquerol, J. Rouquerol and K. Sing, in *Adsorption by Powders and Porous Solids*, Academic Press, London, 1999, pp. 441-442.
28 (*a*) S. Ungureanu, M. Birot, G. Laurent, H. Deleuze, O. Babot, B. Julián-López, M.-F. Achard, M. I. Popa, C. Sanchez and R. Backov, *Chem. Mater.*, 2007, **19**, 5786–5796; (*b*) S. Ungureanu, M. Birot, L. Guillaumme, H. Deleuze, O. Babot, M.-F. Achard, M. I. Popa, C. Sanchez and R. Backov, *Colloids Surf., A*, 2010, **360**, 85–93.
29 M. Joselevich and F. J. Williams, *Langmuir*, 2008, **24**, 11711–11717.
30 S.-Y. Lee, Y. B. Hahn, K. S. Nahm and Y.-S. Lee, *Polym. Adv. Technol.*, 2005, **16**, 328–331.
31 C. Wang, Y. Zhang, H. S. Seng and L. L. Ngo, *Biosens. Bioelectron.*, 2006, **21**, 1638–1643.
32 D. Dattilo, L. Armelao, G. Fois, G. Mistura and M. Maggini, *Langmuir*, 2007, **23**, 12945–12950.
33 H. El Rassy and A. C. Pierre, *J. Non-Cryst. Solids*, 2005, **351**, 1603–1610.
34 E. Pigois, D. Gayot, M. Delamar, M. Leclerc and M. M. Chehimi, *J. Electron Spectrosc. Relat. Phenom.*, 1990, **53**, 79–86.
35 (*a*) C. Schomburg, M. Wark, Y. Rohlfing, G. Schulz-Ekloff and D. Wöhrle, *J. Mater. Chem.*, 2001, **11**, 2014–2021; (*b*) F. M. Raymo, S. Giordani, A. J. P. White and D. J. Williams, *J. Org. Chem.*, 2003, **68**, 4158–4169; (*c*) J. T. C. Wojtyk, A. Wasey, N.-N. Xiao, P. M. Kazmaier, S. Hoz, C. Yu, R. P. Lemieux and E. Buncel, *J. Phys. Chem. A*, 2007, **111**, 2511–2516.
36 A. Shumburo and M. C. Biewer, *Chem. Mater.*, 2002, **14**, 3745–3750.
37 B. C. Bunker, B. I. Kim, J. E. Houston, R. Rosario, A. A. Garcia, M. Hayes, D. Gust and S. T. Picraux, *Nano Lett.*, 2003, **3**, 1723–1727.
38 M. Ehrl, F. W. Deeg, C. Bräuchle, O. Franke, A. Sobbi, G. Schulz-Ekloff and D. Wöhrle, *J. Phys. Chem.*, 1994, **98**, 47–52; M. Bockstette, D. Wöhrle, I. Braun and G. Schulz-Ekloff, *Microporous Mesoporous Mater.*, 1998, **23**, 83–96.
39 W. J. Albery, P. N. Bartlett, C. P. Wilde and J. R. Darwent, *J. Am. Chem. Soc.*, 1985, **107**, 1854–1858.
40 J. Samuel, M. Ottolenghi and D. Avnir, *J. Phys. Chem.*, 1992, **96**, 6398–6405.
41 J. Biteau, F. Chaput and J. P. Boilot, *Mol. Cryst. Liq. Cryst.*, 1997, **297**, 49–56.

 